Technion - Israel Institute of Technology

Advanced Topics in Missile Guidance (088759)

- Final Project -

Influence of the Missile's Wing Configuration upon the Guidance Performance

Prof. Tal Shima

Submitted by : Daniel Engelsman

July 16, 2018

Contents

List of Figures

1 Introduction

In this project I will examine the influence of the missile's wing arrangement (front / rear) on its guidance performances, through different guidance methods (PN, APN and OGL).

As shown, there are 2 admissible formations that satisfy the missile's steering. θ denotes the angle w.r.t inertial horizon and δ is the servo's deflection :

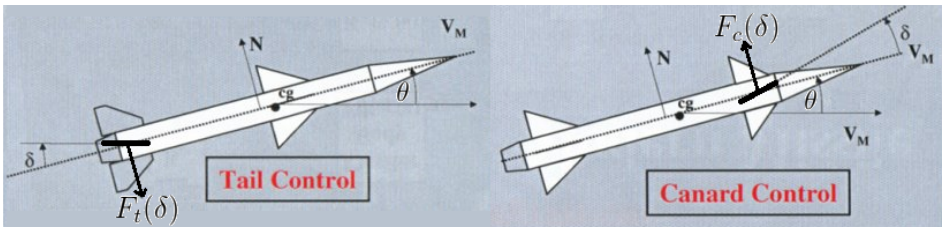

Figure 1: **Left** : Rear wing. **Right** : Front wing.

Symmetry conditions has been proved at both configurations (see **Appendix**), meaning that the **cg** is exactly in the middle of the missile, for clarity purposes.

The airfoils using for steering derive their operation from the coming airflow, and are bounded between maximal angle of attack.

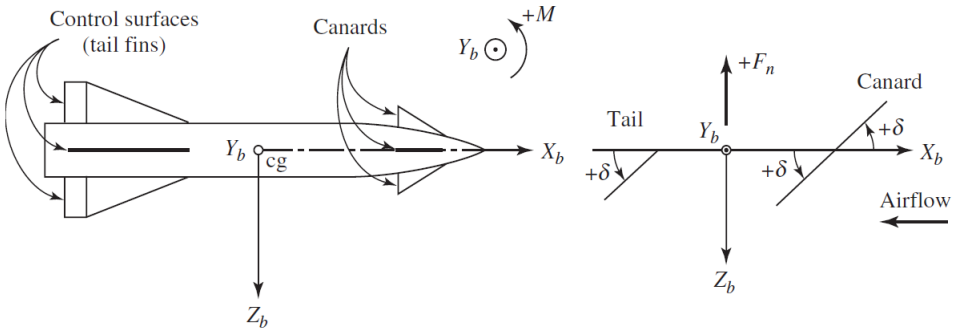

Figure 2: Tail fin and Canard installation

Dynamically speaking, the body angle (θ) is translated into poles on Root Locus, and the servo deflection (δ) into the zeros.

In this project I will analyze the effects of (inner $G_M(s)$) Auto-Pilot on the guidance control (outer loop), and see back and forth how one's design influences the other.

Assumptions Made

- α - Angle of attack, and δ - Servo deflection, are approximated as small angles.
- Longitudinal velocity (V_M) is constant, allowing us discussing only latteral manuevers.
- The missile's center of pressure **coincides** with the center of gravity. The missile's motion is given by **thrust**, and **lift** uses only for manuevering.
- No aerodynamic Effects - In order to keep the problem at a reasonable order (n $\leq$ 3), one must ignore extreme atmospheric effects upon the missile. Hence, $\alpha \approx 0$ all along analysis process. It is of course similar to missiles in outer space, where only rigid body dynamics govern. Therefore, Angle Of Attack (α) can be neglected and we get $\theta = \cancelto{0}{\alpha} + \gamma$, where θ is w.r.t inertial horizon, and γ is the body angle.
- $\theta \leq 90$ to ensure one constant reference frame along analysis.
- $\dot{r}_{cg} = 0$: Center of gravity location remains constant, despite using solid propellant.
- **Guidance** is implemented after 1st order **linearization** of the **kinematics**.

List of Abbreviations

AP	Autopilot
APN	Augmented Proportional Navigation
DGL	Differential Game Law
MD	Miss Distance
NMD	Normalized Miss Distance
MP	Minimum Phase
NMP	Non Minimum Phase
PN	Proportional Navigation
SR	Step Response
Vc	Closing Speed
ZEM	Zero Effort Miss

1.1 Reverse Engineering

As an Ex-commander of Spike (Hebrew: "Gil") missile launching unit, I wanted to make the analysis on that familiar missile, for which I know some "inside info" about his performances.

However, that would be unrealistic since its range and top speed are much less than that of an airplane, and is not really designated to chase after a manuevering target. Therefore, I chose to concentrate on "Python 5" RAFAEL's Air-to-Air Missile (AAM), and extract mechanical details over the internet ("Leaks") and integrate in the dynamic model.

1.2 Missile's Parameters Extraction

Total Weight : 105 kg. Length : 3.1 m Diameter : 0.16 m [2, 3]

Top speed : Mach 4 @ altitude of 40,000 feet equals 1200 $[\frac{m}{sec}]$. [1, 3].

Thrust : 2810 lbf = 12.5 kN @ Double Base Solid Propellant. [4]

1.3 Target's Parameters

Let us consider a standard fighter aircraft that like **F-16** or **F-22** whose capable evading in several g's maneuver. Later on we will see more explicitly the different maneuver scenarios the target will perform, and its influence on the miss distance results.

2 Mathematical Model

Let us present the 2 optional configurations :

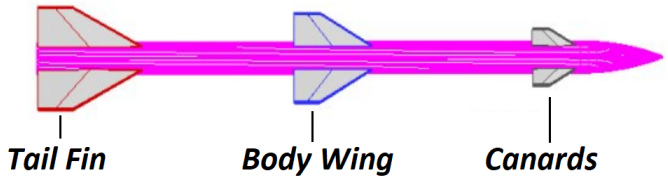

Figure 3: The Auto-Pilot dynamics and its correlated $G_M(s)$

During steady motion, the following analysis exists :

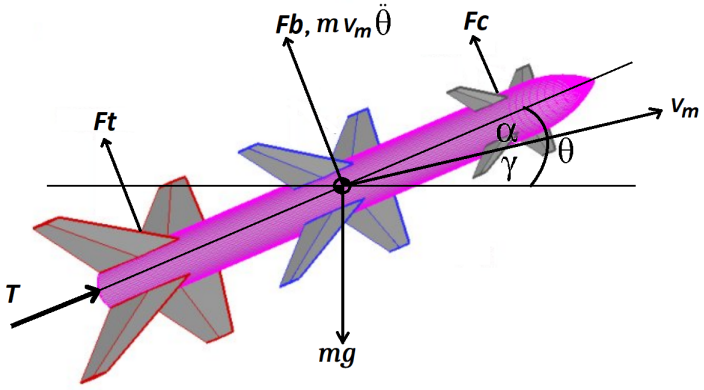

Figure 4: The Auto-Pilot dynamics and its correlated $G_M(s)$

As assumed before, for the sake of simplicity, no aerodynamic effects take place ($\alpha \simeq 0$), and both airfoils are located symmetrically at an equal distance from the **c.g** :

$$\|r_c F_c(\delta)\| = \|r_t F_t(\delta)\| \qquad ; \qquad F_i = \pm\frac{1}{2}\rho V_M^2 S C_\delta \cdot \delta \tag{2.1}$$

Sum of moments from **c.g** :

$$\Sigma M_i = \pm r_i F_i = \pm I_y \ddot{\theta} \qquad ; \qquad I_{cylinder} = \frac{1}{12} M l^2 \quad [\hat{\theta}] \tag{2.2}$$

$$\ddot{\theta} = \frac{r_i \cdot F_i}{I_y} = \frac{r_i \cdot \frac{1}{2}\rho V_M^2 S C_\delta}{\frac{1}{12} M L^2} \cdot \delta = (\frac{6 r_i \cdot \rho V_M^2 S C_\delta}{M l^2}) \cdot \delta \quad \Rightarrow \quad \ddot{\theta} = \pm M_\delta \cdot \delta \tag{2.3}$$

Plug numbers into parameters

Let us now plug the numbers in Eq. (2.3) :

$r_i = 1.25[m]$ $\quad$ $\rho(h = 40,000\ [ft]) = 0.3[\frac{kg}{m^3}]$ $\quad$ $V_M = 1,200\ [\frac{m}{sec}]$ $\quad$ $S = 0.02\ [m^2]$

$C_{\delta,symmetric} = 3.82$ $\quad$ $M = 105[kg]$ $\quad$ $l = 3.1[m]$ $\quad \Rightarrow \quad$ $M_\delta = \pm 245.3\ [sec^{-2}]$

The ($\pm$) sign denotes the current configuration (NMP, MP).

3 AP Control Design

Hereby is the Auto-Pilot (AP) dynamics in Simulink. The are 2 kinds of feedback gains (K - regular $K_{\dot{\theta}}$ - rate), and (ϕ_c, ϕ) are the tail / canard angle w.r.t inertial horizon.

$$G_M(s) = \frac{Ks^2 + KM_\delta}{\tau s^3 + (1+K)s^2 + k_{\dot{v}}M_\delta s + KM_\delta}$$

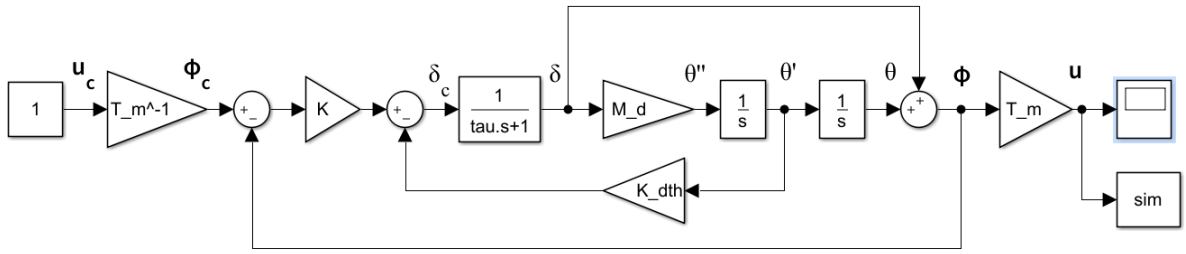

Figure 5: The Auto-Pilot dynamics and its correlated $G_M(s)$ above

Note : At the **Appendix**, one can find the optimization process made for stabilizing the AP controllers. However, at the end I got the following values : $K_{\dot{\theta}} = \pm 0.05$; $K = \pm 0.2$.

MP - Positive values and **NMP** - Negative values. Mind the symmetry conditions that **exist** between both configurations.

3.1 Tail configuration

The original transfer function of the NMP dynamics is : $G_M(s) = \frac{-0.25s^2+50}{0.05s^3+0.75s^2+10s+50}$

By using Matlab's reduced order approximation tools [6, 7], we'll get :

$$G_{M,2nd}(s) = \frac{-8s+106}{s^2+7.515s+106} \quad and \quad G_{M,1st}(s) = \frac{-0.1s+1}{s+1}$$

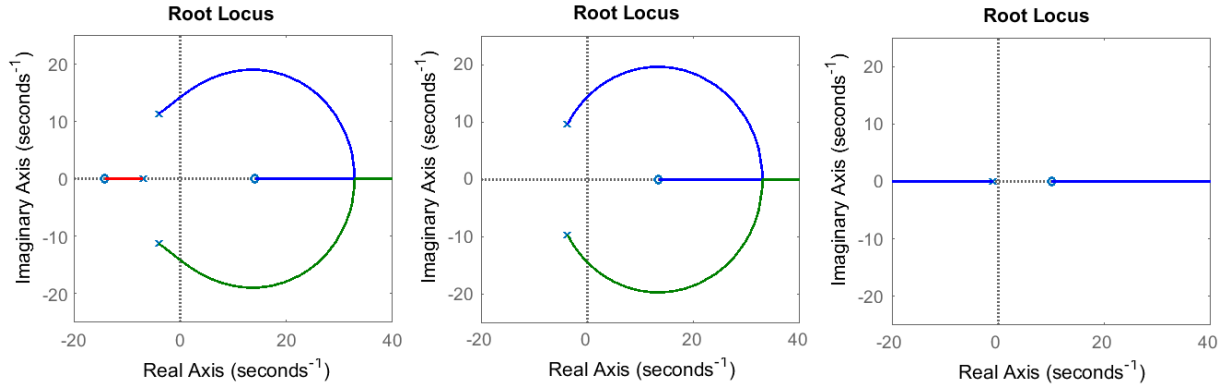

Figure 6: Root Locus diagram of the reduced orders (3rd, 2nd, 1st)

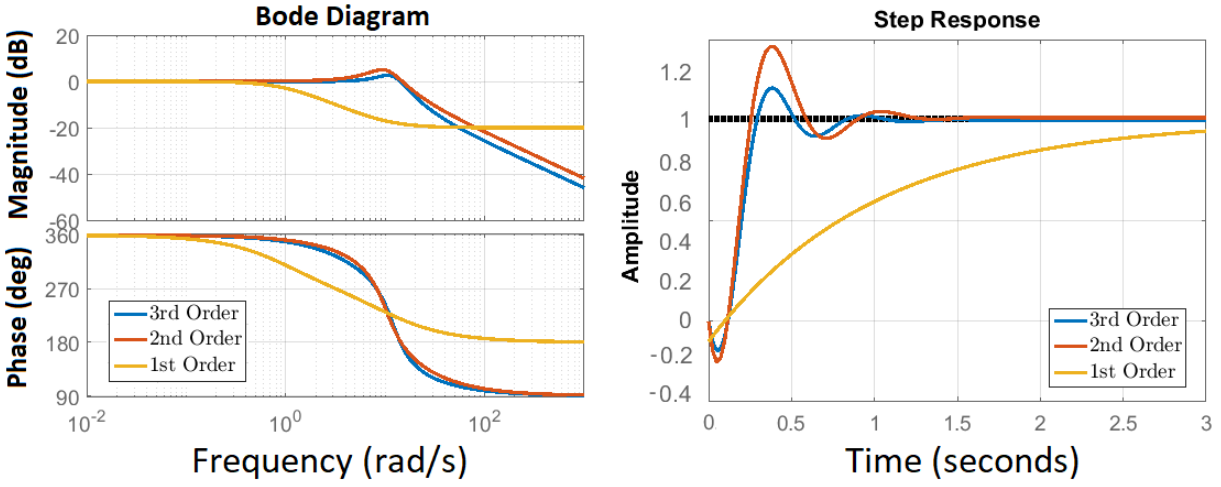

Figure 7: Dynamic properties of the NMP reduced transfer function

Note : One can tell that NMP has an **inverse response**, that later on will be examined.

3.2 Canard configuration

The original transfer function of the MP dynamics is : $G_M(s) = \frac{0.25s^2+50}{0.05s^3+1.25s^2+10s+50}$

By using Matlab's reduced order approximation tools, we'll get :

$$G_{M,2nd}(s) = \frac{1.88s+22.5}{s^2+4.1s+22.5)} \quad and \quad G_{M,1st}(s) = \frac{0.1s+1}{s+1}$$

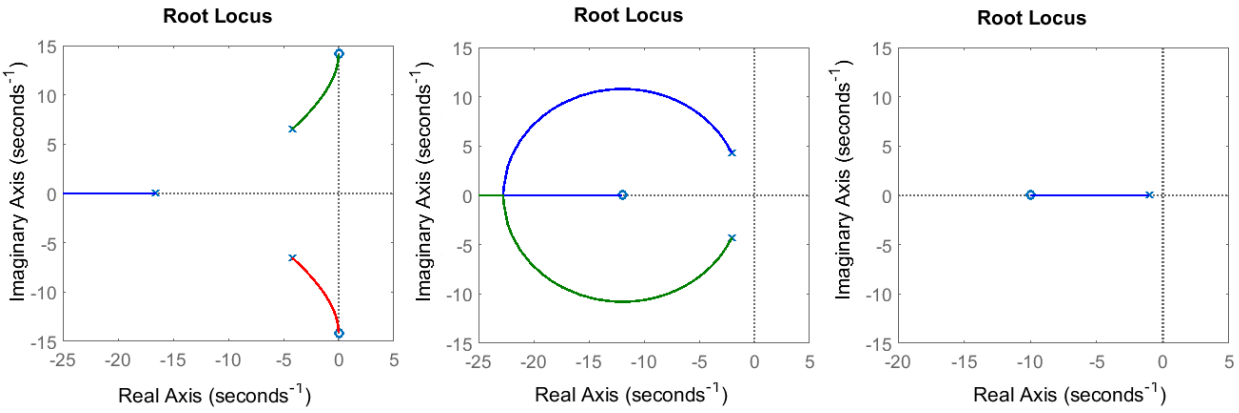

Figure 8: Root Locus diagram of the reduced orders (3rd, 2nd, 1st)

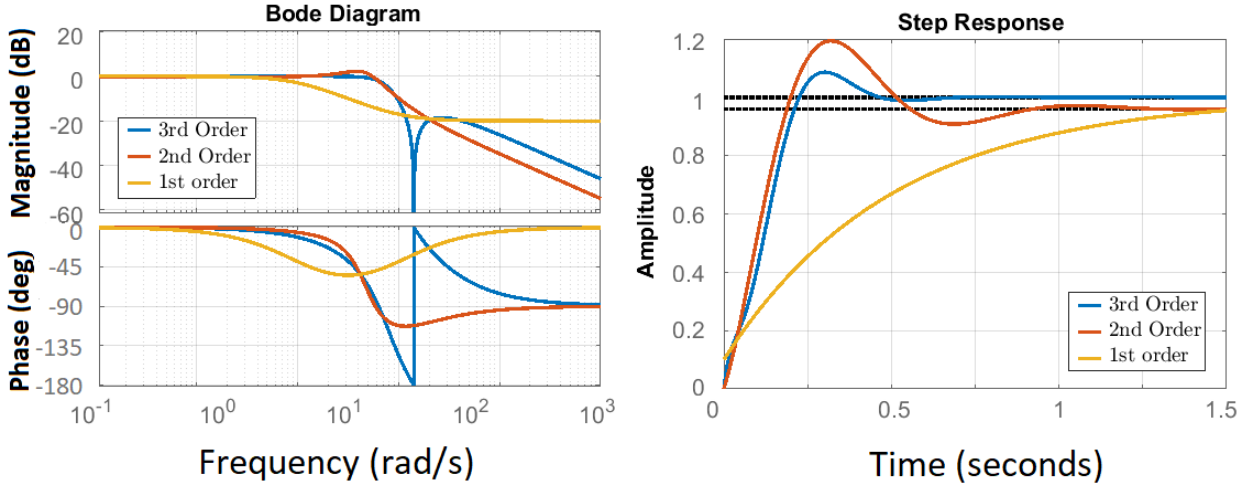

Figure 9: Dynamic properties of the MP reduced transfer function

We can see that altogether, both configurations' reduction, manage to keep a reasonably similar bandwidth at low frequencies, where the servo's operation range works.

Note : Unlike NMP, the MP has a **direct** positive response towards the rise direction.

3.3 State Space Presentation

By reducing the dynamics to 1st order transfer functions, we get the general forms :

$$G_M(s) = \frac{u}{u_c} = \frac{\pm\tau_z s + 1}{\tau_p s + 1} \quad and \quad G_T(s) = \frac{v}{v_c} = \frac{1}{\tau_T s + 1} \qquad \bullet\,(\pm) \quad \equiv \quad \textbf{phase type}. \tag{3.1}$$

An expected obstacle when developing $G_M(s)$, is that $\tau_z s$ in the numerator derives $u_c \Rightarrow \dot{u}_c$ and is no longer valid to be used in a state space form. We will therefore define an auxiliary variable, that will help us neglect $\dot{u}_c$ influence : • $d_M = \frac{\tau_z}{\tau_p} \simeq 0.1$

$$G_M(s) = \frac{u}{u_c} = \frac{d_M\tau_p s + 1}{\tau_p s + 1} \Rightarrow \frac{d_M\tau_p s + 1 + d_M - d_M}{\tau_p s + 1} \Rightarrow \frac{d_M(\tau_p s + 1) + 1 - d_M}{\tau_p s + 1} \tag{3.2}$$

$$G_M(s) = \frac{u}{u_c} = \cancelto{0}{d_M} + \frac{1 - d_M}{\tau_p s + 1} \simeq \frac{1 - d_M}{\tau_p s + 1} \quad \Rightarrow \quad \dot{u} = -(\frac{1}{\tau_p})u + (\frac{1 - d_M}{\tau_p})u_c$$

Our dynamic system can be expressed in a state space form : $\dot{\bar{x}} = A\bar{x} + Bu_c + Cv_c$

$$\dot{x} = \begin{bmatrix} \dot{y} \\ \ddot{y} \\ \dot{u} \\ \dot{v} \end{bmatrix} = \begin{bmatrix} 0 & 1 & 0 & 0 \\ 0 & 0 & 1 & -1 \\ 0 & 0 & -\frac{1}{\tau_p} & 0 \\ 0 & 0 & 0 & -\frac{1}{\tau_T} \end{bmatrix} \begin{bmatrix} y \\ \dot{y} \\ u \\ v \end{bmatrix} + \begin{bmatrix} 0 \\ 0 \\ \frac{1-d_M}{\tau_p} \\ 0 \end{bmatrix} u_c + \begin{bmatrix} 0 \\ 0 \\ 0 \\ \frac{1}{\tau_T} \end{bmatrix} v_c \tag{3.3}$$

The transition matrix : (• $\theta_p = \frac{t_{go}}{\tau_p}$ • $\theta_T = \frac{t_{go}}{\tau_T}$ • $\psi(\zeta) = e^{-\zeta} + \zeta - 1$)

$$\Phi(t_f, t) = \mathcal{L}^{-1}\{(sI - A)^{-1}\} \Leftrightarrow e^{A \cdot t_{go}} = \begin{bmatrix} 1 & t_{go} & -\tau_p^2\psi(\theta_p) & \tau_T^2\psi(\theta_T) \\ 0 & 1 & \tau_p(e^{-\theta_p} - 1) & -\tau_T(e^{-\theta_T} - 1) \\ 0 & 0 & e^{-\theta_p} & 0 \\ 0 & 0 & 0 & e^{-\theta_T} \end{bmatrix} \tag{3.4}$$

Defining the Zero-Effort-Miss (ZEM) term :

$$ZEM = M \cdot \Phi(t_f, t) \cdot \bar{x}(t) = x_1(t) + x_2(t)t_{go} - \tau_p^2\psi(\theta_p)x_3(t) + \tau_T^2\psi(\theta_T)x_4(t) \tag{3.5}$$

4 Developing Optimal Guidance Law

The performance index that is usually chosen for guidance problem is one in which we make the miss zero subject to minimizing the integral of the square of acceleration.

Generally :

$$min\big\{J = h(x(t_f)) + \int_0^{t_f} g(x,u,t)\big\} \tag{4.1}$$

Here,

$$J = \frac{b}{2}y^2(t_f) + \frac{1}{2}\int_0^{t_f} \gamma u_c^2 dt \qquad \Rightarrow \qquad J = \frac{b}{2}x_1^2(t_f) + \frac{1}{2}\int_0^{t_f} \gamma u_c^2 dt \tag{4.2}$$

$$where \qquad h(x(t_f)) = \frac{1}{2}bx_1^2(t_f) \qquad and \qquad g(x,u,t) = \frac{1}{2}\gamma u_c^2 \tag{4.3}$$

Hamiltonian :

$$H(x,\lambda^T,u_c,t) = g(x,u_c,t) + \lambda^T f(x,u_c,t) \quad where \quad f(x,u_c,t) = \dot{x} \tag{4.4}$$

Here,

$$H = \frac{\gamma}{2}u_c^2 + \lambda_1 x_2 + \lambda_2(x_3 - x_4) + \lambda_3 \cdot (\frac{u_c(1-d_M) - x_3}{\tau_p}) + \lambda_4 \cdot (\frac{v_c - x_4}{\tau_T}) \tag{4.5}$$

$\dot{\bar{\lambda}}$ and its boundary conditions for $\bar{\lambda}(t_f)$:

$$\dot{\bar{\lambda}} = \begin{bmatrix}\dot{\lambda}_1\\ \dot{\lambda}_2\\ \dot{\lambda}_3\\ \dot{\lambda}_4\end{bmatrix} = -\frac{\partial \bar{H}}{\partial x_i} = \begin{bmatrix}-\frac{\partial H}{\partial x_1}\\ -\frac{\partial H}{\partial x_2}\\ -\frac{\partial H}{\partial x_3}\\ -\frac{\partial H}{\partial x_4}\end{bmatrix} = \begin{bmatrix}0\\ -\lambda_1\\ -\lambda_2 + \frac{\lambda_3}{\tau_p}\\ \lambda_2 + \frac{\lambda_4}{\tau_T}\end{bmatrix} \quad and \quad \bar{\lambda}(t_f) = \frac{\partial h}{\partial x_f} = \begin{bmatrix}bx_1(t_f)\\ 0\\ 0\\ 0\end{bmatrix}$$

Integrating $\bar{\lambda}_i$ variables, and we get :

$$\lambda_1(t) = \int_0^t \cancelto{0}{\dot{\lambda}_1}\, dt = K \quad \Rightarrow \quad \lambda_1(t_f) = K = bx_1(t_f); \quad \Rightarrow \quad \underline{\underline{\lambda_1(t) = bx_1(t_f)}}$$

$$\lambda_2(t) = \int_0^t \cancelto{-\lambda_1}{\dot{\lambda}_2}\, dt = \int_0^t -bx_1(t_f)\ dt = -bx_1(t_f)t + K \quad \Rightarrow \quad \lambda_2(t_f) = 0 \Rightarrow K = bx_1(t_f)t_f$$

$$\underline{\underline{\lambda_2(t) = bx_1(t_f)(t_f - t)}}$$

$$\dot{\lambda}_3 - \frac{1}{\tau_p}\lambda_3 = -\lambda_2 \quad \Rightarrow \quad (\mu\lambda_3)' = -\mu\lambda_2 \setminus \cdot \int_0^t \quad \Rightarrow \quad \lambda_3 = -e^{\frac{t}{\tau_p}} bx_1(t_f) \int_0^t e^{-\frac{t}{\tau_p}}(t_f - t)dt$$

$$\lambda_3(t) = -e^{\frac{t}{\tau_p}}(bx_1(t_f)\tau_p^2 e^{-\frac{t}{\tau_p}}(\frac{t_f - t}{\tau_M} + 1) + K) \quad \Rightarrow \quad \lambda_3(t_f) = 0 \quad \Rightarrow \quad K = -e^{-\frac{t_f}{\tau_p}}\tau_p^2 bx_1(t_f)$$

$$\lambda_3(t) = -\tau_p^2 bx_1(t_f)(e^{-\frac{t_f - t}{\tau_p}} + \frac{t_f - t}{\tau_p} + 1) = -\tau_p^2 bx_1(t_f)(e^{-\theta_p} + \theta_M - 1)$$

$$\underline{\underline{\lambda_3(t) = -\tau_p^2 bx_1(t_f)\psi(\theta_p)}}$$

$$\dot{\lambda}_4 - \frac{1}{\tau_T}\lambda_4 = \lambda_2 \quad \Rightarrow \quad (\mu\lambda_4)' = \mu\lambda_2 \setminus \cdot \int_0^t \quad \Rightarrow \quad \lambda_4 = e^{\frac{t}{\tau_T}} bx_1(t_f) \int_0^t e^{-\frac{t}{\tau_T}}(t_f - t)dt$$

$$\lambda_4(t) = e^{\frac{t}{\tau_T}}(bx_1(t_f)\tau_T^2 e^{-\frac{t}{\tau_T}}(\frac{t_f - t}{\tau_T} + 1) + K) \quad \Rightarrow \quad \lambda_4(t_f) = 0 \quad \Rightarrow \quad K = e^{-\frac{t_f}{\tau_T}}\tau_T^2 bx_1(t_f)$$

$$\lambda_4(t) = -\tau_T^2 bx_1(t_f)(e^{-\frac{t_f - t}{\tau_T}} + \frac{t_f - t}{\tau_T} + 1) = -\tau_T^2 bx_1(t_f)(e^{-\theta_T} + \theta_T - 1)$$

$$\underline{\underline{\lambda_4(t) = \tau_T^2 bx_1(t_f)\psi(\theta_T)}}$$

And the Optimal Guidance control is defined as :

$$u^* = \frac{\partial H}{\partial u_c^*} = \gamma u_c + \lambda_3 \frac{(1 - d_M)}{\tau_p} = 0 \quad \Rightarrow \quad u_c^* = -\frac{\lambda_3}{\gamma\tau_p}\psi(\theta_p)$$

$$u_c^* = \frac{b}{\gamma}x_1(t_f)\tau_p(1 - d_M)\psi(\theta_p) \quad \Rightarrow \quad \underline{\underline{u_c^* = (\frac{b}{\gamma})x_1(t_f)(\tau_p - \tau_z)\psi(\theta_p)}} \tag{4.6}$$

Calculating the general case for $x_1(t_f)$, using $\mathrm{M} = [1\ \ 0\ \ 0\ \ 0]^T$:

$$\begin{aligned} x_1(t_f) &= \Phi(t_f,t)\bar{x}(t) + \int \Phi(t_f,t)B\cdot u_c^*(\zeta)\ \ d\zeta + \int \Phi(t_f,t)C\cdot v_c(\zeta)\ \ d\zeta \\ &= ZEM - \tau_p^2\frac{(1-d_M)}{\tau_p}(\frac{b}{\gamma})x_1(t_f)(\tau_p-\tau_z)\int \psi^2(\theta_p)\ \ d\zeta + (\frac{1}{\tau_T})\tau_T^2\int \psi(\theta_T)v_c(\zeta)\ \ d\zeta \\ &= ZEM - x_1(t_f)\cdot(\frac{b}{\gamma})(\tau_p-\tau_z)^2\int \psi^2(\theta_p)\ \ d\zeta + \tau_T\int \psi(\theta_T)v_c(\zeta)\ \ d\zeta \end{aligned}$$

We'll use the following short-cut:

$$W = \int \psi^2(\theta_p)\ \ d\zeta = \frac{\tau_p}{6}\cdot(2\theta_p^3 - 6\theta_p^2 + 6\theta_p - 12\theta_p e^{-\theta_p} - 3e^{-2\theta_p} + 3) \tag{4.7}$$

$$v_c(t)\neq 0 \quad \Rightarrow \quad Q = \int \psi(\zeta)\ \ d\zeta = \left[\psi(\frac{t_f-\zeta}{\tau_p})\right|_t^{t_f} = -\tau_T[\psi(\theta_T) - \frac{1}{2}\theta_p^2] \tag{4.8}$$

And finally we get :

$$x_1(t_f) = \frac{ZEM + \tau_T\int \psi(\theta_T)v(\zeta)\ \ d\zeta}{1+(\frac{b}{\gamma})(\tau_p-\tau_z)^2\int \psi(\theta_p)^2\ \ d\zeta} = \underline{\underline{\frac{ZEM + \tau_T\int \psi(\theta_T)v_c(\zeta)\ \ d\zeta}{1+(\frac{b}{\gamma})(\tau_p-\tau_z)^2\cdot W}}} \tag{4.9}$$

Optimal Guidance Control

$$u_c^* = (\frac{b}{\gamma})(\tau_p-\tau_z)\psi(\theta_p)\cdot\left[\frac{ZEM + \tau_T\int \psi(\theta_T)v_c(\zeta)\ \ d\zeta}{1+(\frac{b}{\gamma})(\tau_p-\tau_z)^2\cdot W}\right] \tag{4.10}$$

Later on we will examine the different cases for u_c^* and see what parameters are most influential at each scenario.

Effective Navigation Ratio

For simplicity we'll present N'_{OGL} as follows :

$$N'(\theta_p) = \underline{\underline{\frac{\tau_p^2(\frac{b}{\gamma})(\tau_p-\tau_z)\cdot\theta_p^2\cdot\psi(\theta_p)}{1+(\frac{b}{\gamma})(\tau_p-\tau_z)^2\cdot W(\theta_p)}}} \tag{4.11}$$

Let us present the $N'(\theta_p)$ behaviour under 2 different γ weight functions :

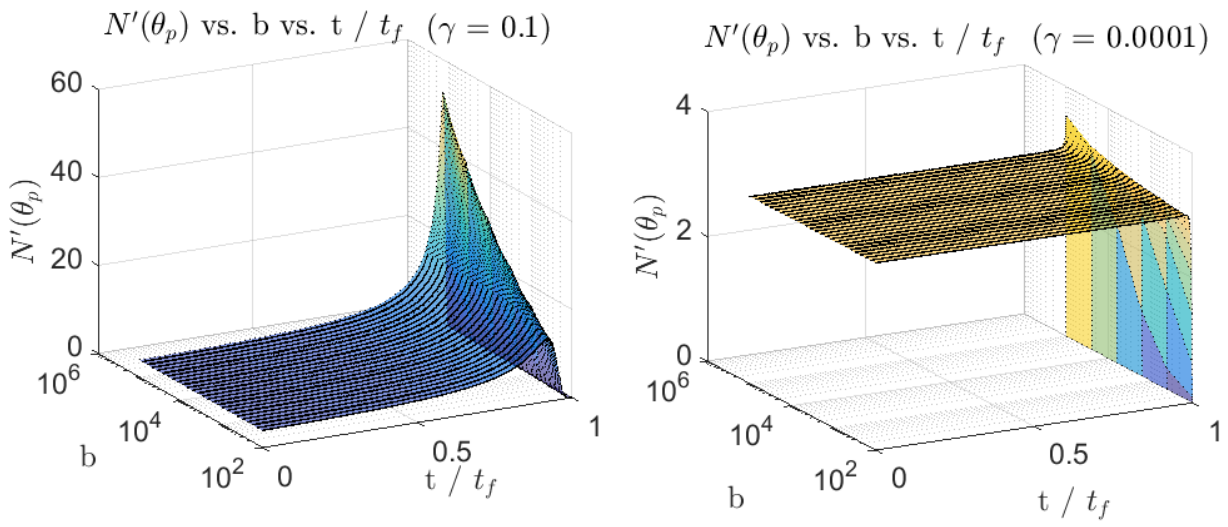

Figure 10: Sensitivity of $N'(\theta)$ to parameters

One can see that when b and γ are small, so does the required $N'(\theta)$. But when they both grow, the control effort rises respectively. In addition, we can see that $N'(\theta)$ starts at $N'(\theta) \simeq 3$ (like PN/APN) and along the flight time rises towards a local peak.

Project Objectives

After developing the mathematical grounds for the project, hereby is the content. Along the project I will **compare** the performances of both **Tail** and **Canard** configurations, under 3 guidance laws and through 3 different cases of the target's behaviour :

Target Maneuver	$v_c(t)$	Guidance Law	Configuration
None	$v_c(t) = 0$	PN, APN, OGL	MP vs. NMP
Const.	$v_c(t) = Const.$	PN, APN, OGL	MP vs. NMP
Bang-Bang	$v_c(t) = a_{T,max} \cdot sign(t_{cr})$	PN, APN, OGL	MP vs. NMP
Bang-Bang	a_M^{max} vs. a_T^{max}	DGL/1	MP vs. NMP

Note : When (b, γ) are not stated, the default values were chosen as (b = 1000, $\gamma = 0.1$).

5 No Target Maneuver

When the target does not maneuver we get that $x_4(t) = v_c(t) = 0$. And the rest goes :

$$ZEM_{v=0} = M \cdot \Phi(t_f, t) \cdot \bar{x}(t)_{v=0} = x_1(t) + x_2(t)t_{go} - \tau_p^2 \psi(\theta_p) x_3(t) \tag{5.1}$$

$$u_c^* = \frac{N'(\theta_p)}{t_{go}^2} \cdot ZEM_{v=0} \tag{5.2}$$

The following simulations show how a given parameter is influenced by the phase sign. Note that **all axes** in graphs are **normalized**, and $\tau_z > 0$ denotes MP (Canard) while $\tau_z < 0$ means NMP (Tail). Using the defaults values of (b = 1000, $\gamma = 0.1$) we'll see the following :

Controller Performance

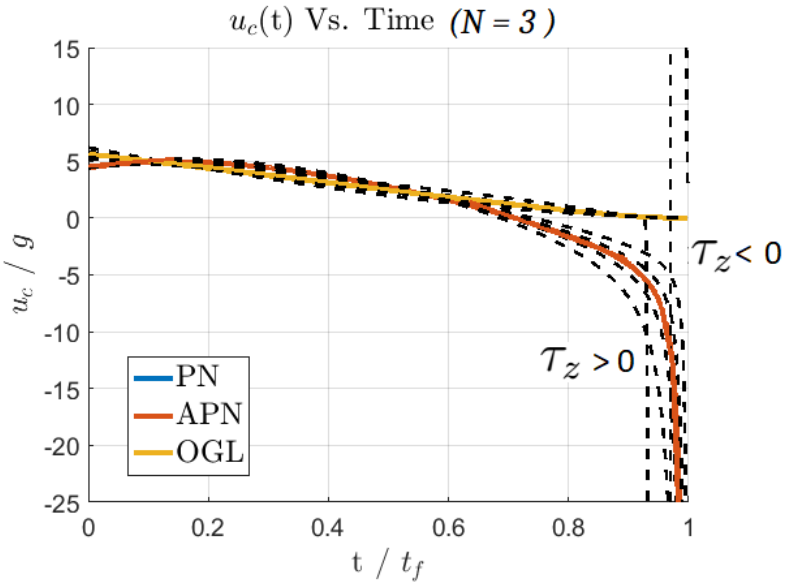

Figure 11: Acceleration Command, $\tau_z \in$ [-0.15 0.15]

Since no target maneuver occur, the PN and APN are converged, and show slight u_c reduction in the MP, meaning it takes less control effort. The OGL shows indifference to the phase sign, but towards the end of the flight time shows small fluctuations.

Normalized $\Delta y(t)$

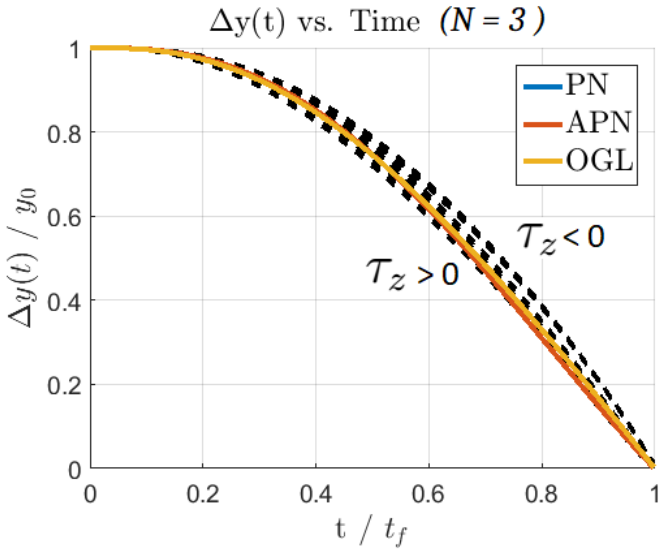

Figure 12: Vertical Distance vs. Flight Time, $\tau_z \in$ [-0.15 0.15]

We can see that MP configuration ($\tau_z > 0$) lowers the trajectory, meaning that it enables higher velocity. On the other hand, the NMP ($\tau_z < 0$) makes a longer arc implying that it has lower velocity. **Note :** $\tau_z = 0$ denotes **neutral** phase $\Leftrightarrow$ regular 1st order without τ_z.

Let us now look at the final values concentrated in the table :

		Guidance Law		
	τ_z	PN	APN	OGL
NMP	-0.15	1.602	1.602	0.313
	-0.1	1.457	1.457	0.285
	-0.05	1.060	1.060	0.278
	0	0.843	0.843	0.271
MP	0.05	0.713	0.713	0.265
	0.1	0.630	0.630	0.259
	0.15	0.574	0.574	0.253

Figure 13: Miss Distance Table

One can tell that no difference exist between PN and APN guidance laws (since v_c=0), and the OGL exhibits better performances. Furthermore, at all methods, there is a diminishing tendency from NMP $\Rightarrow$ MP, giving priority to the canard (MP).

OGL Sensitivity

Now I would like to examine the OGL's sensitivity to the parameters of the navigation ratio. Using the adjoint simulation I will check the normalized MD sensitivity to b and γ :

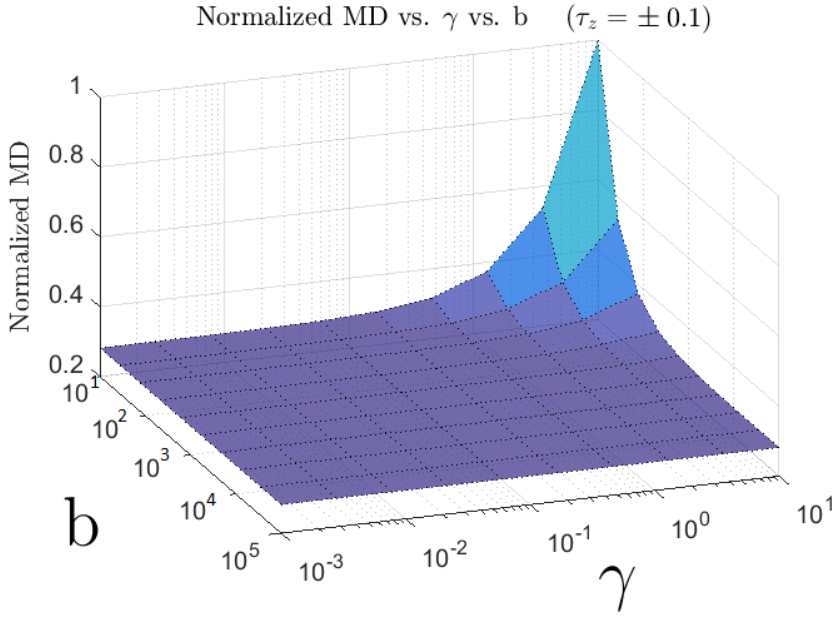

Figure 14: NMD Sensitivity grid to b and γ

We can see that the MD reacts inversely to each of the parameters, due to the weights of the cost function **J** (Eq. 4.2). The sharp reaction occurs at the top right cross section of $(b \downarrow)$ and $(\gamma \uparrow)$. That makes sense because the big weight of γ on the controller u_c, and contrarily the low weight of **b** on $x_1(t_f)$, guarantee poor performances to the interceptor.

6 Constant Target Maneuver

When target performs constant maneuver $v_c(t) = a_T = 3g$, the parameters go as follows:

$$ZEM = M \cdot \Phi(t_f, t) \cdot \bar{x}(t)_{v_c=aT} = \overbrace{x_1(t) + x_2(t)t_{go} - \tau_p^2\psi(\theta_p)x_3(t)}^{\text{ZEM,v=o}} + \tau_T^2\psi(\theta_T)x_4(t)$$
$$ZEM_{v_c=C} = ZEM_{v=0} + \tau_T^2\psi(\theta_T)x_4(t) + \tau_T \int \psi(\theta_T)v_c(\zeta)\ d\zeta \Big|_{v_c=aT} \tag{6.1}$$

And we get the following expression for Zero-Effort-Miss :

$$ZEM_{v_c=aT} = x_1(t) + x_2(t)t_{go} - \tau_p^2\psi(\theta_p)x_3(t) + \tau_T^2\psi(\theta_T)x_4(t) - a_T\tau_T^2[\psi(\theta_T) - \frac{1}{2}\theta_p^2] \tag{6.2}$$
$$ZEM_{v_c=a_T} = x_1(t) + x_2(t)t_{go} - \tau_p^2\psi(\theta_p)x_3(t) + \tau_T^2\psi(\theta_T)(x_4(t) - a_T) + \frac{1}{2}a_T t_{go}^2$$

And the optimal controller at constant maneuever is: $u_c^* = \frac{N'(\theta_p)}{t_{go}^2} \cdot ZEM_{v_c=aT}$

Controller Performance

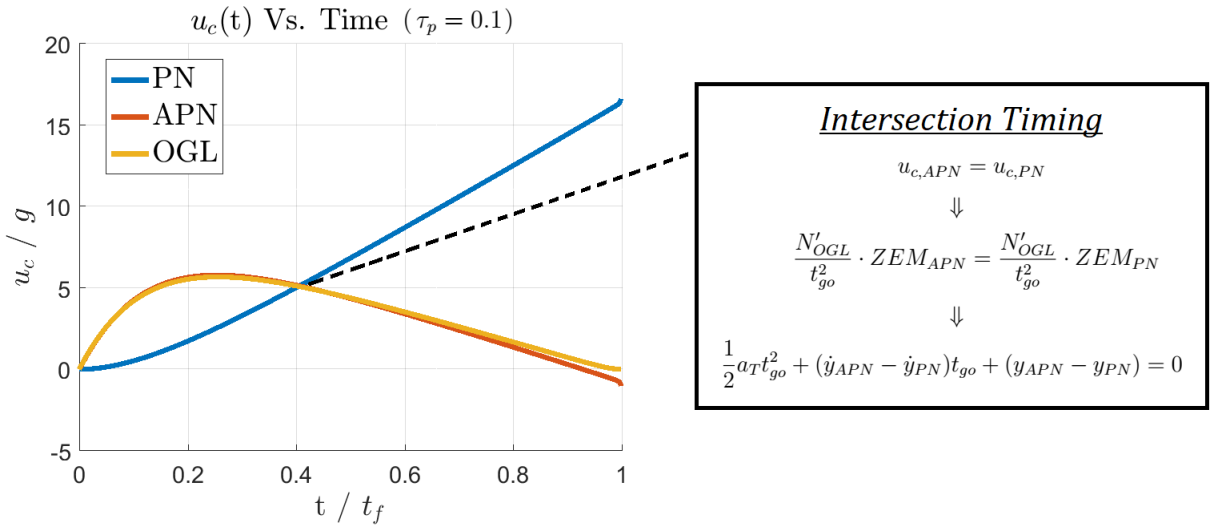

Figure 15: u_c vs. Time, **Neutral** case ($\tau_z = 0$)

Unlike previously, now we can see that PN and APN act entirely different. The OGL almost converges with the APN's u_c. The intersection between PN and APN is explained above. Now, let us examine the phase influence on u_c via $(\tau_z = d_M \cdot \tau_p)$:

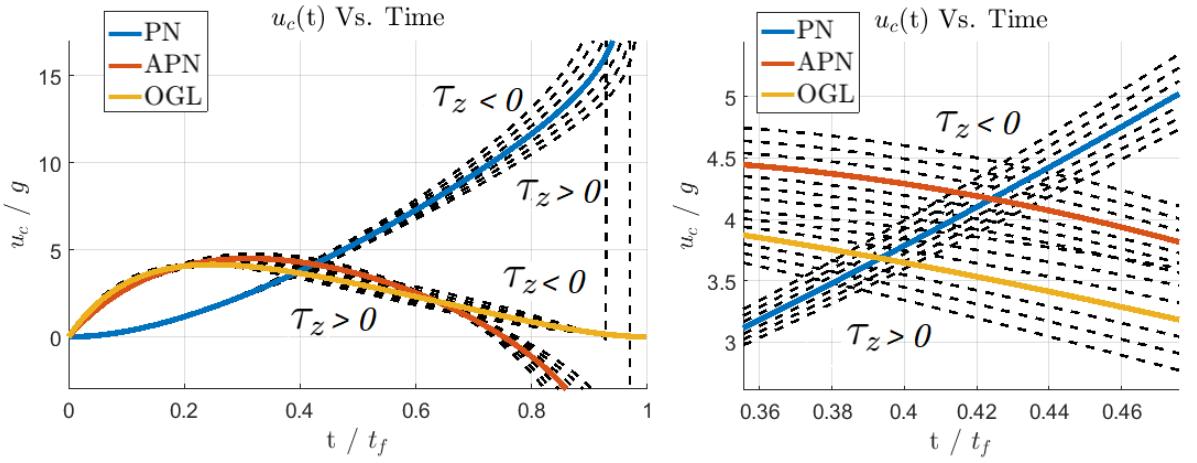

Figure 16: **Left** :u_c vs. Time **Right :** Intersection close-up

This time the influence of τ_z is much stronger on each of the guidance laws. One can tell that NMP ($\tau_z < 0$) configuration requires bigger u_c as opposed to MP ($\tau_z > 0$). But that make sense, since the fact that NMP has an inverse response for every action (**Fig.** 7).

Miss Distance

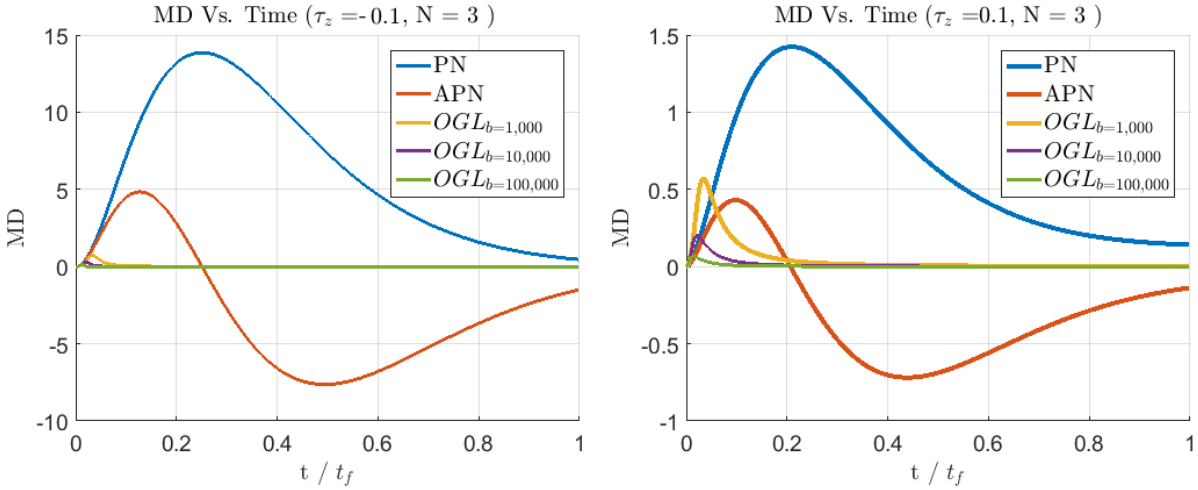

Figure 17: Miss Distance for PN, APN and OGL (γ=0.1)

From the adjoint simulation we can see that the Miss Distance seem alike for both configurations, but differs in the MD magnitude. Both PN and APN exhibit acute reaction to the phase sign, but contrarily the OGL stays almost constant, and reacts mainly to changes in b weight. As expected, the NMP exhibit poor performance in comparison to MP.

OGL Sensitivity

Let us again conduct an optimization process where (b, γ) combine the MD grid. The first simulation is for the Canard (MP), where unlike previously, the target now maneuvers 3g :

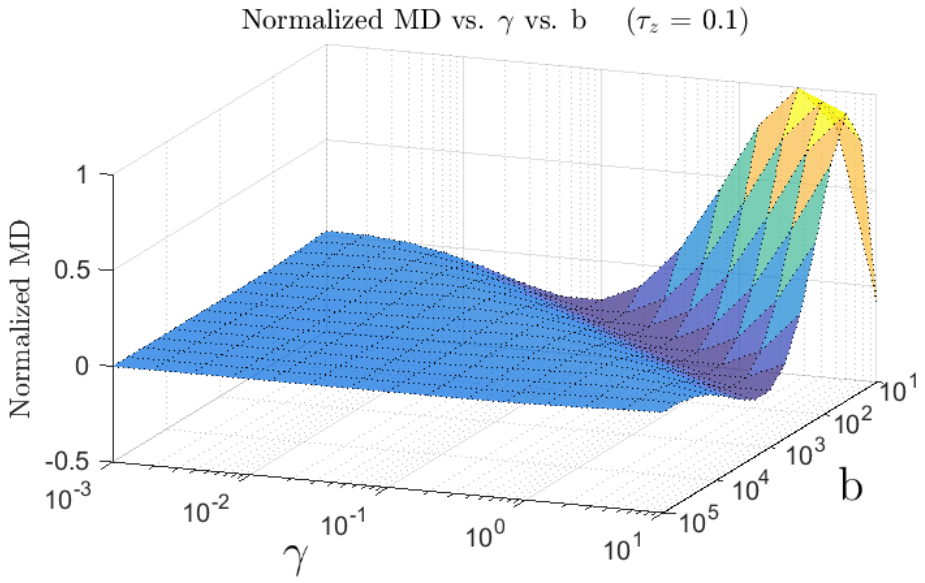

Figure 18: NMD Sensitivity grid @ MP

Again we can see the biggest MD at the top right corner, where ($b \downarrow$ and $\gamma \uparrow$), but there is a lower hall where the Miss Distance turns to be **Negative**. This can be explained by the characteristics of the AP dynamics, which fluctuates along flight time (**Fig.** 17).

However, when the system is (NMP) Tail (**Fig.** 19), it seems somewhat interesting :

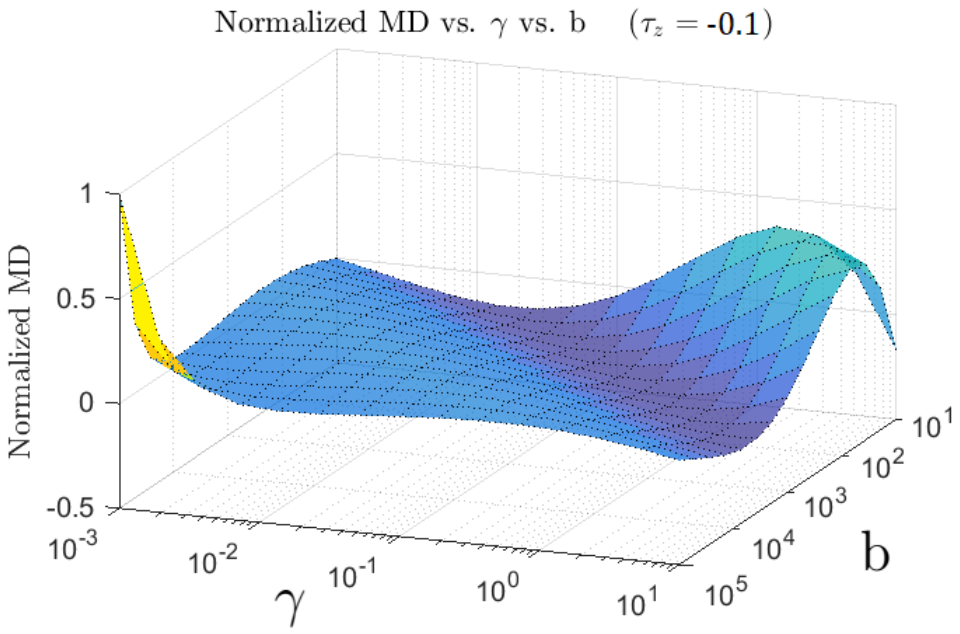

Figure 19: NMD Sensitivity grid @ NMP

Unlike previous results (**Fig.** 18), here we get an opposite results. There is still a sensitivity where ($b \downarrow$ and $\gamma \uparrow$), but contrarily we see the highest MD to the left where ($b \uparrow$ and $\gamma \downarrow$).

At this stage I tried to change the integration step size, the logarithmic range of the parameters, and some initial conditions, but results kept the same.

It is of course rather suspicious, since the both weights ($b \uparrow$ and $\gamma \downarrow$) on the cost function **J** play in favour of the minimum MD. But I decided to show it **although** it is not so explainable.

7 Bang-Bang Meneuver

Similarly to previous chapter yet different, in this scenario the target performs constant maneuver that switches sign randomly every once in a while - $v_c(t) = a_T \cdot sign(t(i) \cdot (-1)^i)$. The vector t(i) is a "time cartridge" that is calculated before execution, and stores the number "N", of the chosen switches : $t(i) = rand([0\ \ 1], N, 1) \cdot t_f$, where $a_T = \pm 3 \cdot g$.

$$
\begin{aligned}
ZEM = M \cdot \Phi(t_f, t) \cdot \bar{x}(t)_{v_c=\pm aT} &= \overbrace{x_1(t) + x_2(t)t_{go} - \tau_p^2 \psi(\theta_p) x_3(t)}^{\text{ZEM,v=o}} + sign(t(i)) \cdot a_T \tau_T^2 \psi(\theta_T) \\
ZEM_{v_c=\pm aT} &= ZEM_{v=0} + \tau_T^2 \psi(\theta_T) x_4(t) + \tau_T a_T \cdot sign(t(i)) \cdot \int \psi(\theta_T)\ d\zeta \\
ZEM_{v_c=\pm aT} &= ZEM_{v=0} + \tau_T^2 \psi(\theta_T) x_4(t) - a_T \tau_T^2 \cdot sign(t(i))[\psi(\theta_T) - \frac{1}{2}\theta_p^2] \qquad (7.1) \\
ZEM_{v_c=\pm a_T} &= ZEM_{v=0} + \tau_T^2 \psi(\theta_T)(x_4(t) - a_T \cdot sign(t(i))) + \frac{1}{2} a_T t_{go}^2 \cdot sign(t(i))
\end{aligned}
$$

And the optimal controller at constant maneuever is: $u_c^* = \frac{N'(\theta_p)}{t_{go}^2} \cdot ZEM_{v_c=\pm aT}$.
Let us first look at the v_c performances under ideal and non ideal dynamics ($a_T = \pm 3g$):

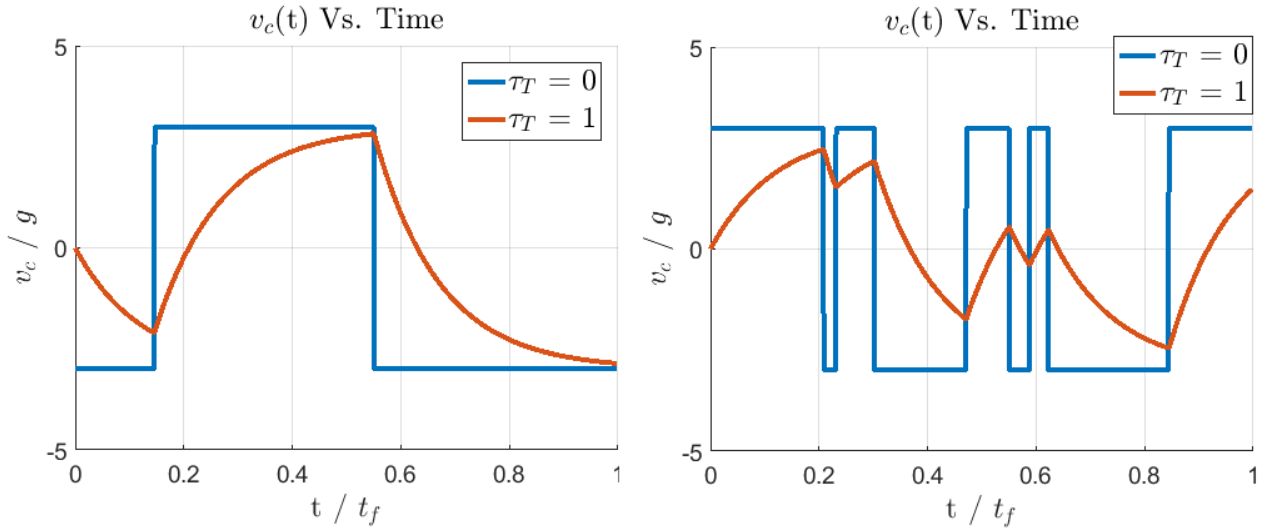

Figure 20: **Left :** $i = 3$ switches **Right :** $i = 9$ switches

We can see that when the number of the random switches grow ($i \uparrow$), the realized target dynamics ($\tau_T > 0$), barely gets to the bounded values, and is thus less effective.

Controller Performance

Note : The controller performance u_c showed slight difference between both configurations, and hence did I unite them into one graph. When the target switches twice, we can see results that slightly resembles the u_c at constant maneuver. PN and APN grow towards end of flight time to $\pm\infty$, while the OGL remains stable.

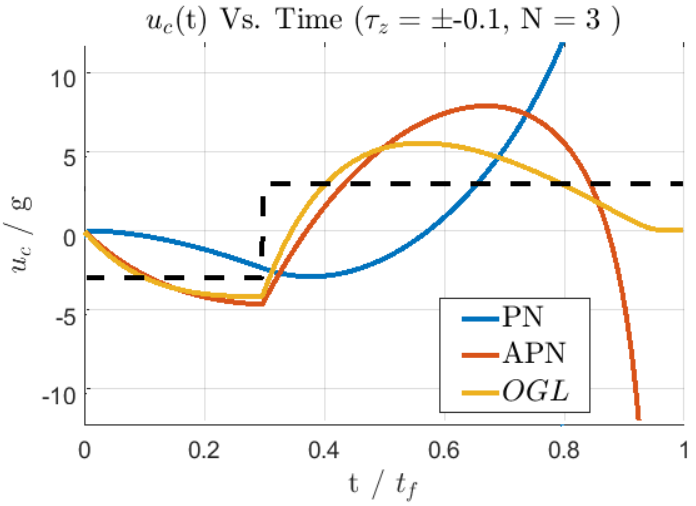

Figure 21: u_c Controller when target switches (i=2)

When the switches number grows, the PN is first to explode into high u_c values, which practically are useless ($\approx 15g$). Contrarily, APN follows OGL until the last switch, before it also approaches $infty$.

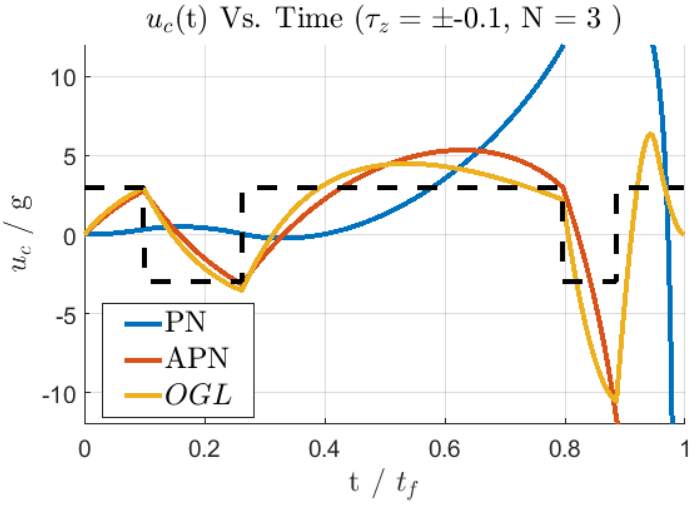

Figure 22: u_c Controller when target switches (i=5)

Now when the target's maneuver becomes more like "fluctuations" all guidance laws are having hard times to keep track, and stay at the bounded hall of $\pm 3g$. The OGL of course does better than PN and APN, but is more vulnerable than before.

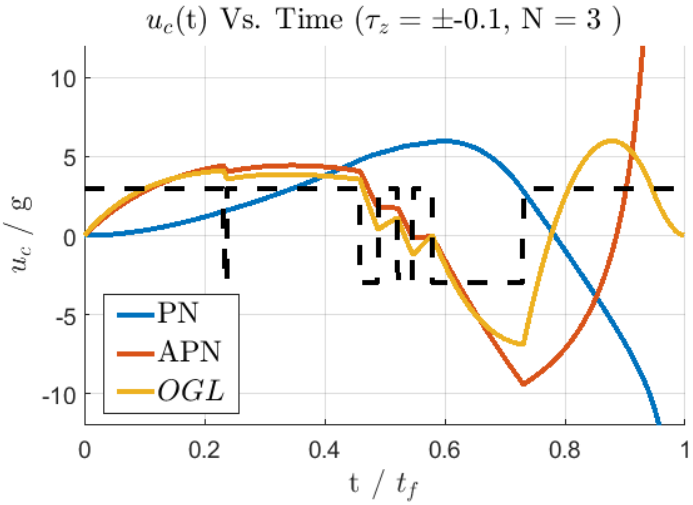

Figure 23: MD when target switches (i=9)

In the next section, we will try to figure out whether the Interception Miss Distance is influenced by the u_c performances we've just seen.

Miss Distance

Unlike u_c, the MD showed an interesting phenomenon - **Extreme** sensitivity to the phase sign, and to the used guidance law. **Note :** *dashed line* denotes switching times.

When the target switches twice, we get normal results almost as seen in simple constant maneuver, where only the phase sign influence. As expected the PN is more vulnerable than APN to the swithcing time along the flight time. The OGL shows almost indifference to the switching time (i=2), and also PN and APN manage to recover.

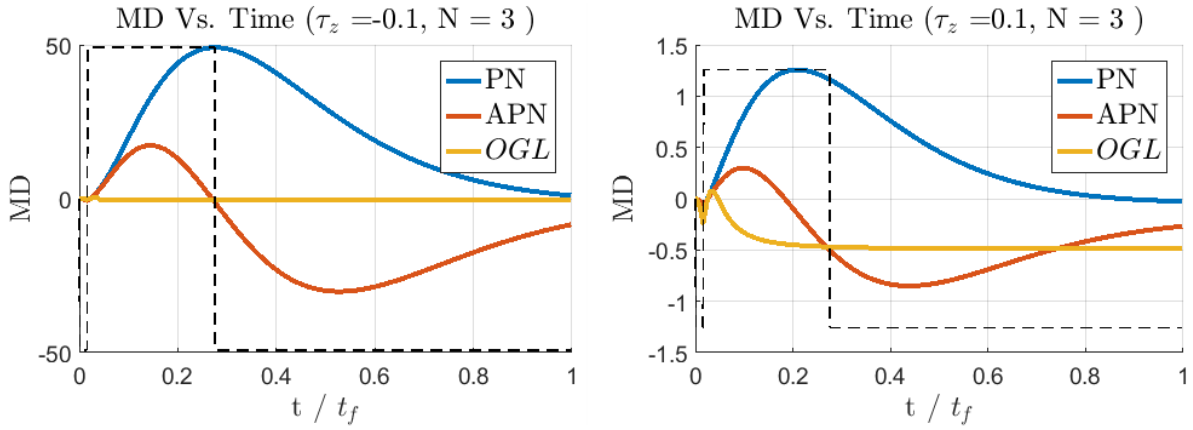

Figure 24: **Left :** NMP Switches (i=2) **Right :** MP

This time we can see that PN and APN diverge at a certain point and start losing effectiveness. Although in MP they get not too far from the OGL performances, in NMP, they *do not even hit the target*. The OGL however, does despite its frequent maneuver.

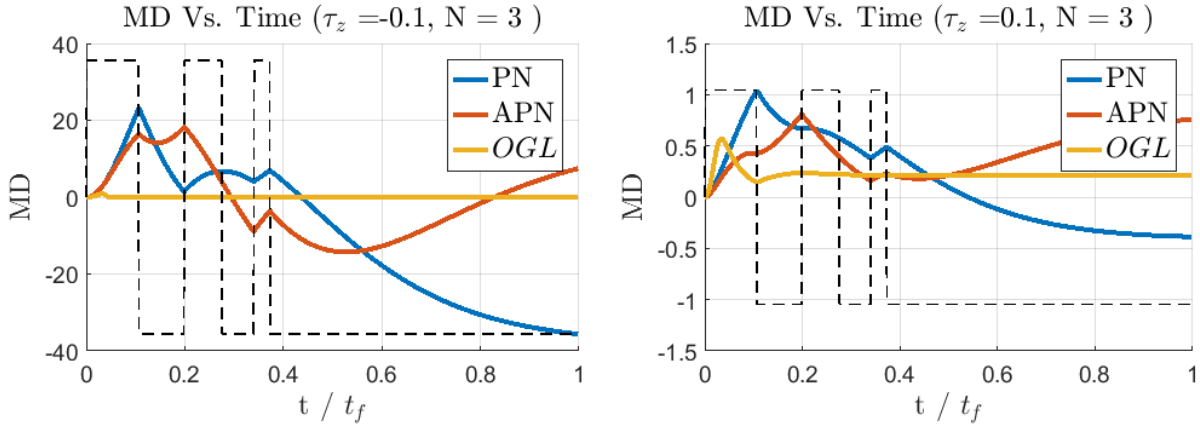

Figure 25: **Left :** NMP Switches (i=5) **Right :** MP

This time, the missile is quite desperate using PN and APN. After several switches they diverge, especially in NMP. An explainable reason is actually from the previous section, where u_c exhibited divergence in PN and APN.

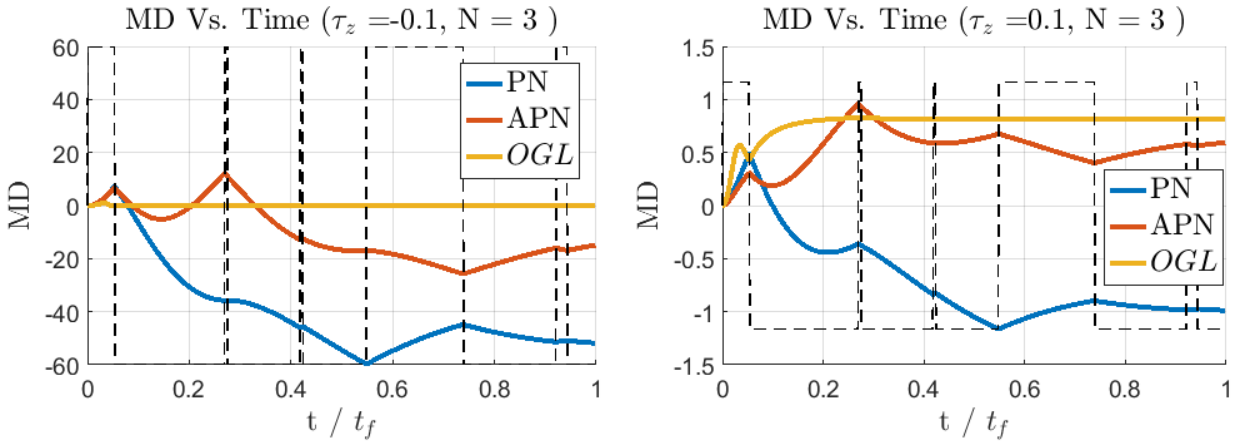

Figure 26: **Left :** NMP Switches (i=9) **Right :** MP

OGL Sensitivity

Let us conduct again the OGL Normalized Miss Distance sensitivity grid to (b, γ) parameters, whereas in the first simulation the target switches 3 times :

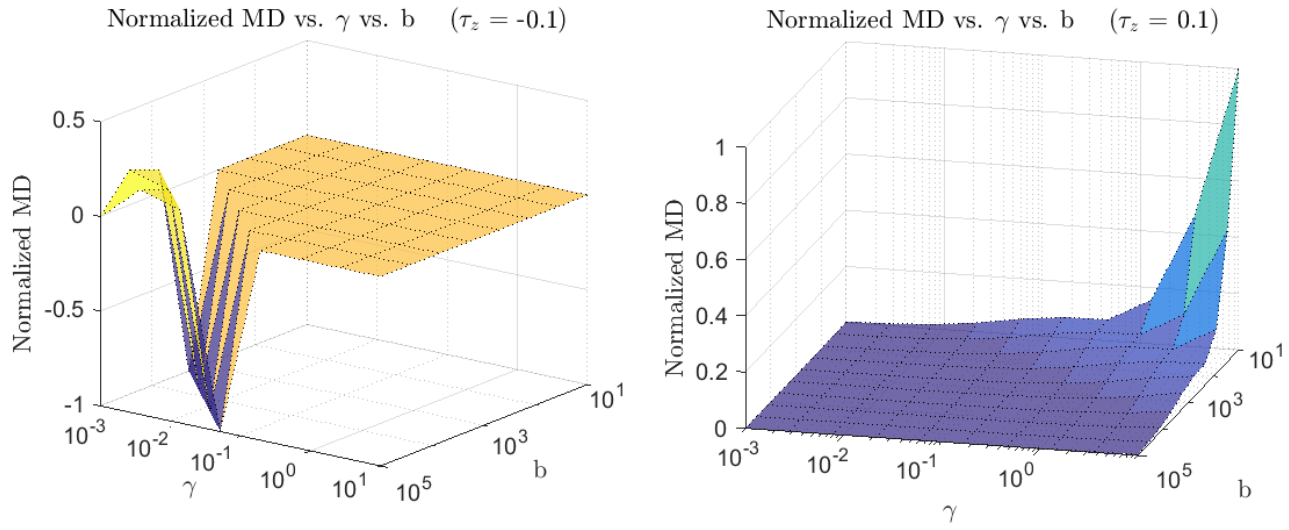

Figure 27: **Left :** NMP Switches (i=3) **Right :** MP

Quite as before, we get the same distribution of high NMD when ($b \downarrow$ and $\gamma \uparrow$) from the same reasons of the weights upon **J**.

Now we shall check what happens when the target "fluctuates" 9 times along flight time :

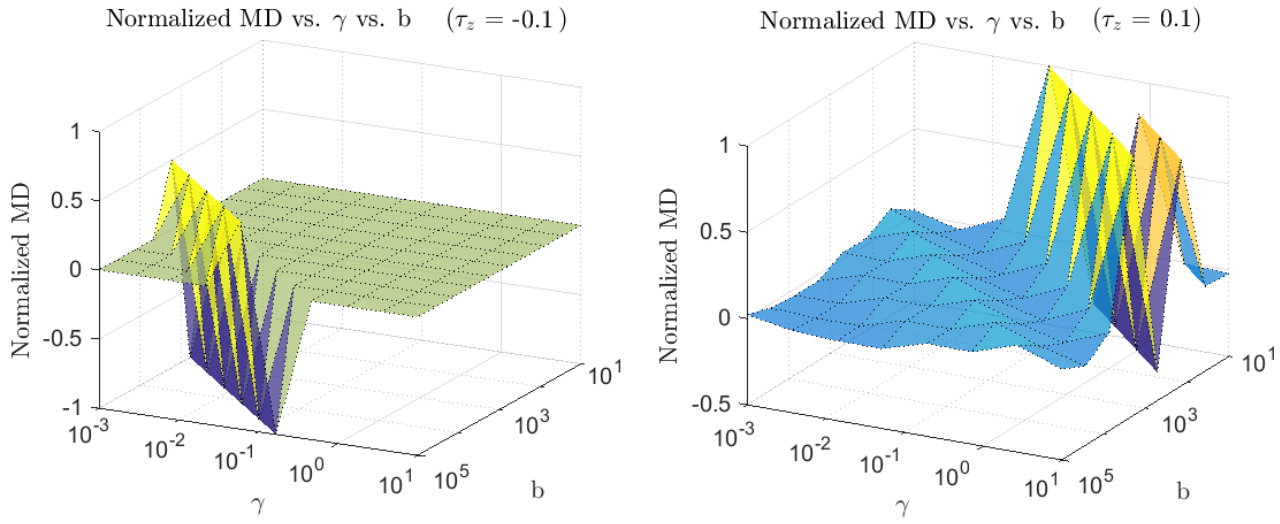

Figure 28: **Left :** NMP Switches (i=9) **Right :** MP

Again, as in (**Fig.**19), we can see that the NMP exhibit opposite reaction to the MP, and we get the highest miss when ($b \uparrow$ and $\gamma \downarrow$).

Furthermore, there is an interesting distribution of several zones where the OGL exhibits sensitivity, and will get poor capture, at each of the configuration.

The possible explanation for the wave-like manifold, is the presence of τ_z in u_c expression (**Eq.** 4.10) changing sign along flight time.

8 Differential Game Theory

After seeing the interceptor-target reciprocal under the former cost function (**Eq.** 4.2), I would like now to consider a 2 sided conflict with both having 1st order dynamics (DGL/1).

The controllers are at maximum capability (saturated), meaning :

$$u_c \Rightarrow u_c a_M^{max} \qquad where \qquad u_c \leq 1 \tag{8.1}$$

$$v_c \Rightarrow v_c a_T^{max} \qquad where \qquad v_c \leq 1 \tag{8.2}$$

$$Dynamics: \quad \tau_p = \tau_T = 1 \qquad Acc. \quad ratio: \qquad \mu = \frac{a_M^{max}}{a_T^{max}} > 1 \tag{8.3}$$

Under the same procedure shown at (**Eq.** 3.2), we get the following ZEM:

$$Z(t_{go}) = M \cdot \Phi(t_f, t) \cdot \bar{x}(t) = x_1(t) + x_2(t) t_{go} - \tau_p^2 \psi(\theta_p) u + \tau_T^2 \psi(\theta_T) v \tag{8.4}$$

And its derivative :

$$\dot{Z}(t_{go}) = M(\dot{\Phi}(t_f, t)x + \Phi(t_f, t)\dot{x}) = M\Phi(t_f, t)(B(t_f, t)u_c + C(t_f, t)v_c) \tag{8.5}$$

$$\dot{Z}(t_{go}) = -\tau_p \psi(\theta_p)(1 - d_M) u_c a_M^{max} + \tau_T \psi(\theta_T) v_c a_T^{max} \tag{8.6}$$

$$Short - cut: \qquad \tilde{\chi}_i(t_f, t) = M\Phi(t_f, t)\chi_i(t_f, t) \tag{8.7}$$

The Hamiltonian :

$$H = \lambda_z \dot{Z}(t_{go}) = \lambda_z(\tilde{B}(t_f, t)u_c + \tilde{C}(t_f, t)v_c)$$

$$\dot{\lambda}_z(t_f) = -\frac{\partial H}{\partial Z} = 0, \qquad \lambda_z = sign(z(t_f)) \tag{8.8}$$

The bidirectional differential game is defined such that each side tries to fulfil his interest :

$$u^* = arg_u max(H) = -sign(\tilde{B}(t_f, t) z(t_f)) \tag{8.9}$$

$$v^* = arg_v max(H) = sign(\tilde{C}(t_f, t) z(t_f)) \tag{8.10}$$

And from (**Eq.** 8.6) we get :

$$\tilde{B}(t_f, t) < 0 \qquad and \qquad \tilde{C}(t_f, t) > 0 \quad \Rightarrow \quad u_c^* = v_c^* = sign(z(t_f)) \tag{8.11}$$

So the updated $\dot{Z}(t_{go})$ will be written as :

$$\dot{Z}(t_{go}) = (\psi(\theta_p)(\tau_p - \tau_z)a_M^{max} + \tau_T\psi(\theta_T)a_T^{max})sign(z(t_f)) \tag{8.12}$$

Let us use the following function to calculate the game space over ZEM vs. t_{go} plane :

$$Where \qquad \delta(t_f, t) = \underline{\underline{\tau_T\psi(\theta_T) - \mu\psi(\theta_p)(\tau_p - \tau_z)}} \tag{8.13}$$

Note that all **3 time constants** appear in that function, showing that the development stayed loyal to the idea of the project - pronouncing the dynamics' significance. Additionally, and most meaningful is the **acceleration ratio** μ that decides whether a capture will occur.

Critical Switching Timing

Let us look at the switching t_{cr} that is obtained. **Note :** ($\tau_z < 0$: Tail, $\tau_z > 0$ Canard) :

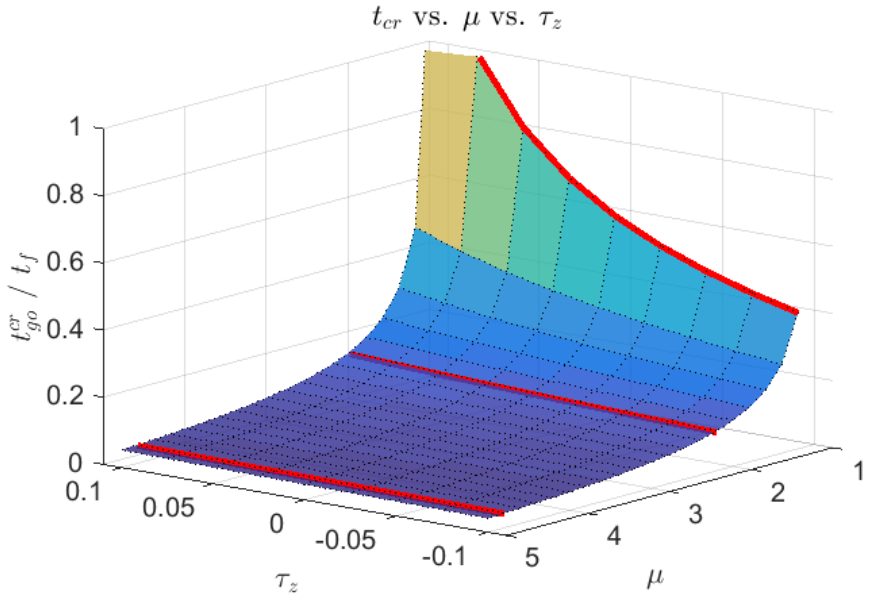

Figure 29: Switching time Matrix

One can tell that when **acceleration ratio** $\mu = 1.1$ is low (**Upper Line**), almost equal, the target is capable to switch / maneuver already at the beginning of the flight time, and by so has greater chances to evade the pursuer. Additionally, the τ_z sign and magnitude changes dramatically at this ratio.

The **Middle line**, denotes $\mu = 2.2$, and we see that the critical timing has been cut off dramatically, and is not more than 15% before $t_{go} = 0$. The target has significantly less time to perform maneuver and enhance the miss distance.

The **Lower line**, which is the highest ratio $\mu = 5$ denotes the poor switching opportunities the target has, and that's only towards end of flight time. Phase sign is almost meaningless.

Game Space Analysis

Let us now examine each of these lines' ZEM ($\mu \in [1.1, 2.2, 5]$) in a game space presentation.

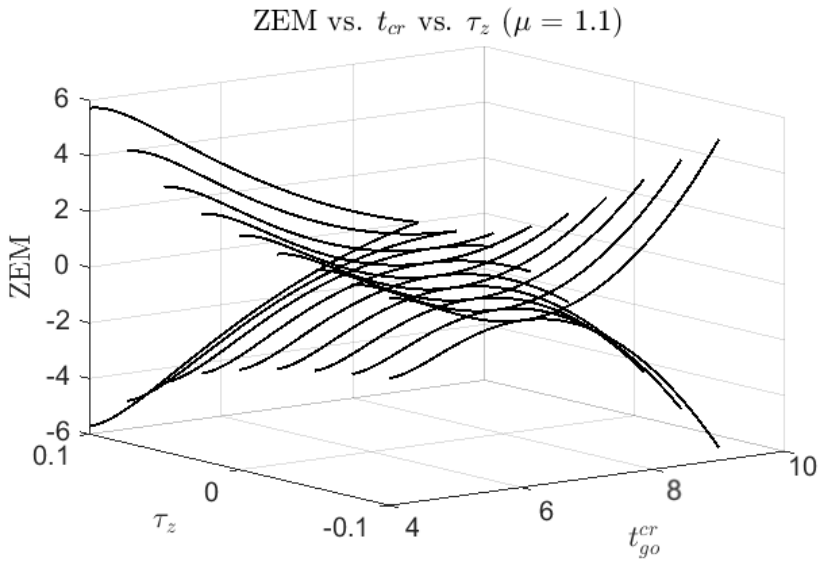

Figure 30: ZEM Game Space ($\mu = 1.1$)

The t_{cr} shows an interesting phenomenon of the switching time which advances from MP to NMP, and shows a dramatic sensitivity to τ_z. **Unlike** what we've so far seen, it is now the Tail showing better performances over the Canard in means of ZEM.

Right to the t_{cr} at each trajectory, there is a singular region that's called **Arbitrary Zone**. Here the interceptor's is able to use simpler guidance laws and reduce control effort until the target reaches t_{cr} and then u_c shall perform **optimal policy**. Here however, that zone is rather small, reflecting the target's agility advantage.

When the acceleration ratio rises, the ZEM is reduced dramatically and is now less influenced by the phase sign. The target's agility almost not exists anymore since it is coerced to perform the maneuver only a moment before capture, in order to evade.

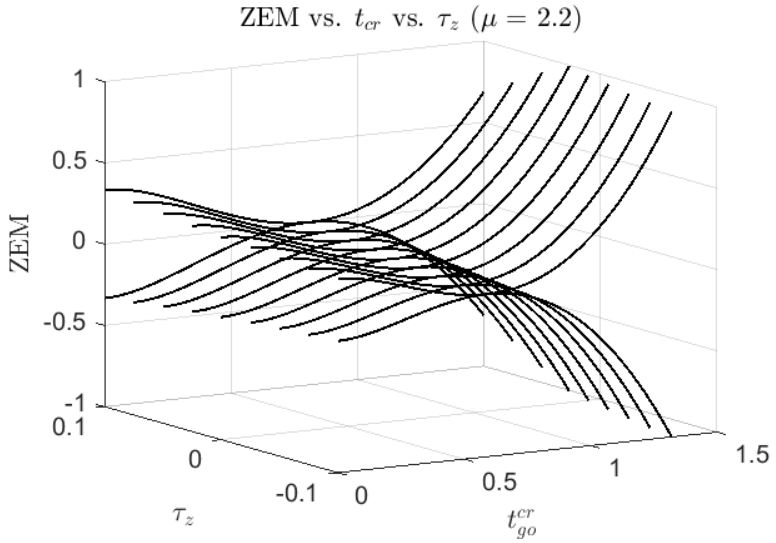

Figure 31: ZEM Game Space ($\mu = 2.2$)

Highest μ ratio shows the pursuer supremacy over the evader, allowing him staying arbitrary most of the flight time. The target seems helpless against such an acceleration ratio, and it is not surprise that the ZEM turns out so small, ensuring lethality of the missile's warhead. Additionally, phase sign is absolutely meaningless, not by sign nor its magnitude.

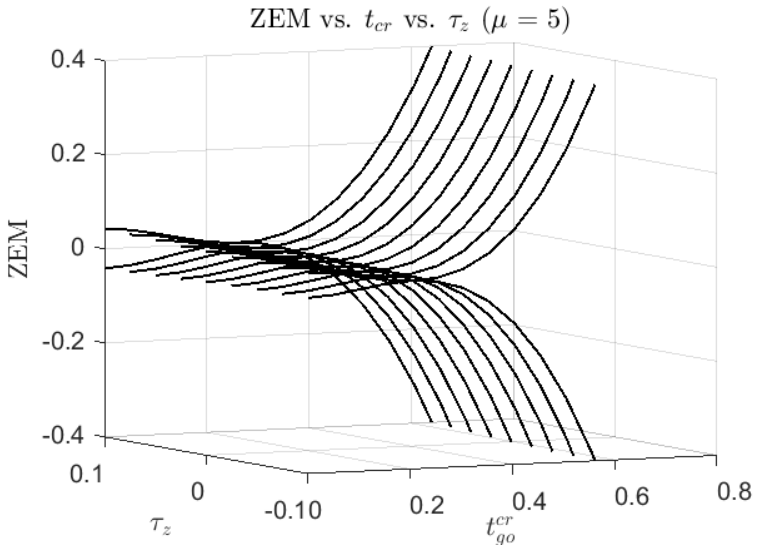

Figure 32: ZEM Game Space ($\mu = 5$)

9 Summary

In this project I have conducted a comprehensive comparison between 3 different guidance laws, in order to examine each one's performances. The early chapters dealt with the PN, APN and OGL development under 3 different scenarios :

Target Maneuver	$v_c(t)$	Guidance Law	Configuration
None	$v_c(t) = 0$	PN, APN, OGL	MP vs. NMP
Const.	$v_c(t) = Const.$	PN, APN, OGL	MP vs. NMP
Bang-Bang	$v_c(t) = a_{T,max} \cdot sign(t_{cr})$	PN, APN, OGL	MP vs. NMP
Bang-Bang	a_M^{max} vs. a_T^{max}	DGL/1	MP vs. NMP

At each chapter I have tried to show an **interesting** 3D graphs in order to demonstrate the significance of **spectral range** per each discussed parameter. Inevitably, there is plenty more other parameters that have been practically ignored.

Main Conclusions

- Vehicle's dynamics play an important role, but capture itself is most influenced by kinematic performances and skilled maneuvers.
- The OGL showed an impressive advantage almost at all scenarios over PN and APN, in means of miss distance and control effort.
- The Canard (MP) showed a notable dominance along early chapters, under PN, APN and OGL Guidance. The NMP's nature to produce **inverse response**, was expectedly harming his performances.
- In DGL/1 - The NMP (Tail) configuration showed better performances in means of homing and ZEM, **unlike** the written above.
- In realistic environment, 1st order reduction will ignore many processes and parameters that at extreme scenarios might be found as crucial.

References

[1] Global Defense Technology Magazine. [Date unknown]. URL: https://defence.pk/pdf/threads/air-forces-air-to-air-missiles-lraam-python-5-industry-rumors.5296.

[2] Pakistan Defence Journal. [May 15 2007]. URL: https://www.airforce-technology.com/projects/python-5-air-to-air-missile-aam-rafael-israel/.

[3] English Wikipedia, Python Missile Article. [Date unknown]. URL: https://en.wikipedia.org/wiki/Python(missile).

[4] PLANE.ORG, Fightsim Community for X-Plane. [Date unknown]. URL: http://www.x-plane.org/home/urf/aviation/text/missiles/aam.html.

[5] Gutman, S., Goldan, O., "Guaranteed Miss Distance in Guidance Systems with Bounded Controls and Bounded Noise". *Journal of Guidance, Control and Dynamics*, Vol. 35, No. 3, May–June 2012.

[6] Varga, A., "Balancing-Free Square-Root Algorithm for Computing Singular Perturbation Approximations," Proc. of 30th IEEE CDC, Brighton, UK (1991), pp. 1062-1065.

[7] D. McFarlane, K. Glover, M. Vidyasagar, "Reduced-order controller design using coprime factor model reduction", IEEE Trans. Autom. Contr., vol. AC-35, pp. 369-373, 1990.

[8] Bakshi, V.U.B.U.A., Linear Control Systems, Technical Publications 2007

[9] Zarchan, P., Tactical and Strategic Missile Guidance 2007, American Institute of Aeronautics and Astronautics

[10] N A Shneydor, Missile Guidance and Pursuit: Kinematics, Dynamics and Control, [1 Jan 1998], Elsevier.

Appendix - Controllers Tuning

In this appendix I will show how did I tuned the state and rate feedback controllers shown at **Fig.** 5 of the 3rd order dynamics. Let us consider the following matrix presenting a family of the AP step responses (SR). We can see a rapid divergence at the right top corner.

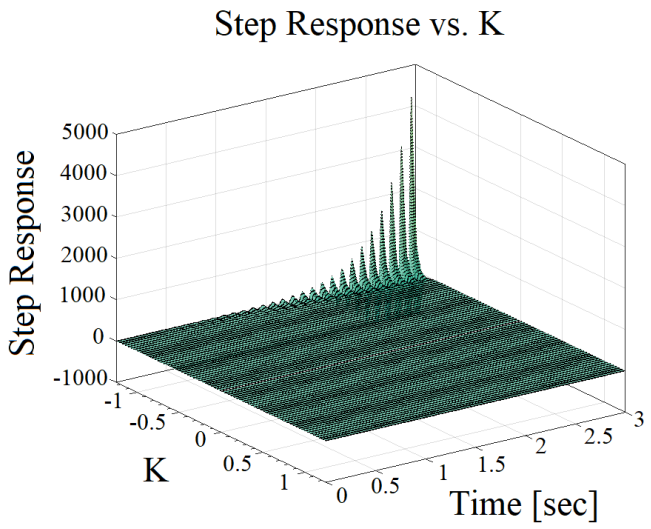

Figure 33: Step Response Matrix for $K_{\dot{\theta}} = \pm 1$

We can see Thousands % deviation. Therefore let us narrow K range in half :

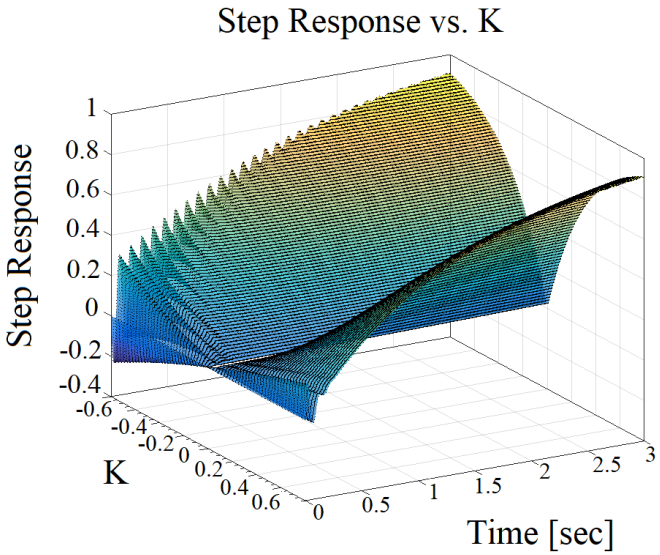

Figure 34: Step Response Matrix for $K_{\dot{\theta}} = \pm 1$

Definitely useful, as we can see a familiar formation of SR rising towards "1" value. However, one can tell the different behaviours that each side exhibits. The negative (**NMP**) exhibits unstable SR with **spikes** whereas the (**MP**) shows a smoother form.

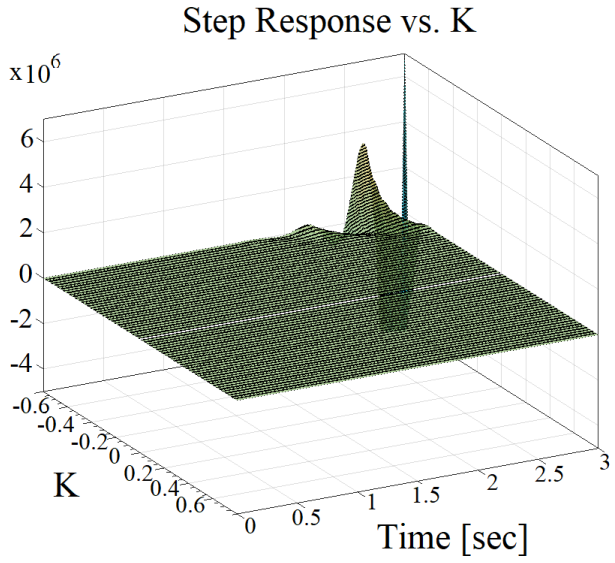

Figure 35: Step response of AP inner loop Vs. $K_{\dot{\theta}} = \pm 0.01$

This time I minimized $K_{\dot{\theta}}$ in order to check the SR matrix. As can be seen, K we once again get a huge unstable "Explosion" at the margins. Therefore, we'll look for a "middle" K value and shorten the time axis towards the desired time frame ($t_r = 10\tau$).

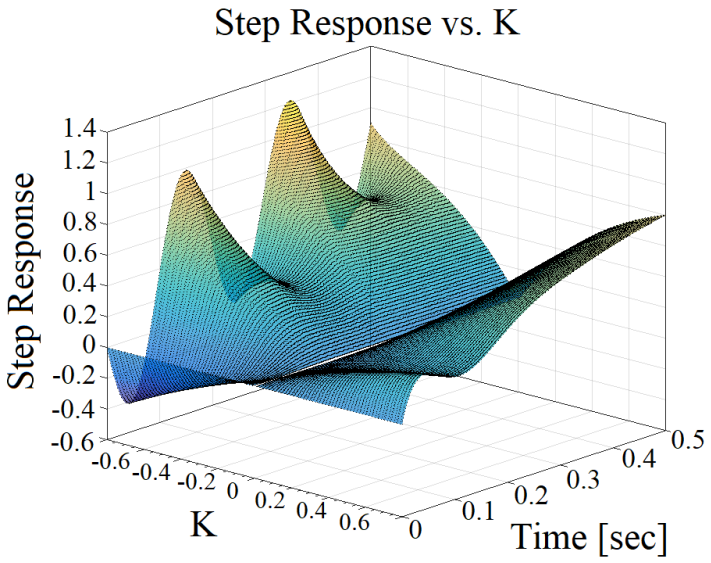

Figure 36: Step response of AP inner loop Vs. $K_{\dot{\theta}} = \pm 0.1$

This time we can see reasonable domain where both **MP** and **NMP** are getting towards "1" in almost 90 % of the t_r. However, the **NMP** still exhibits unstable behaviour that's characterized by undesired fluctuations. Let us reduce once again $K_{\dot{\theta}}$ values.

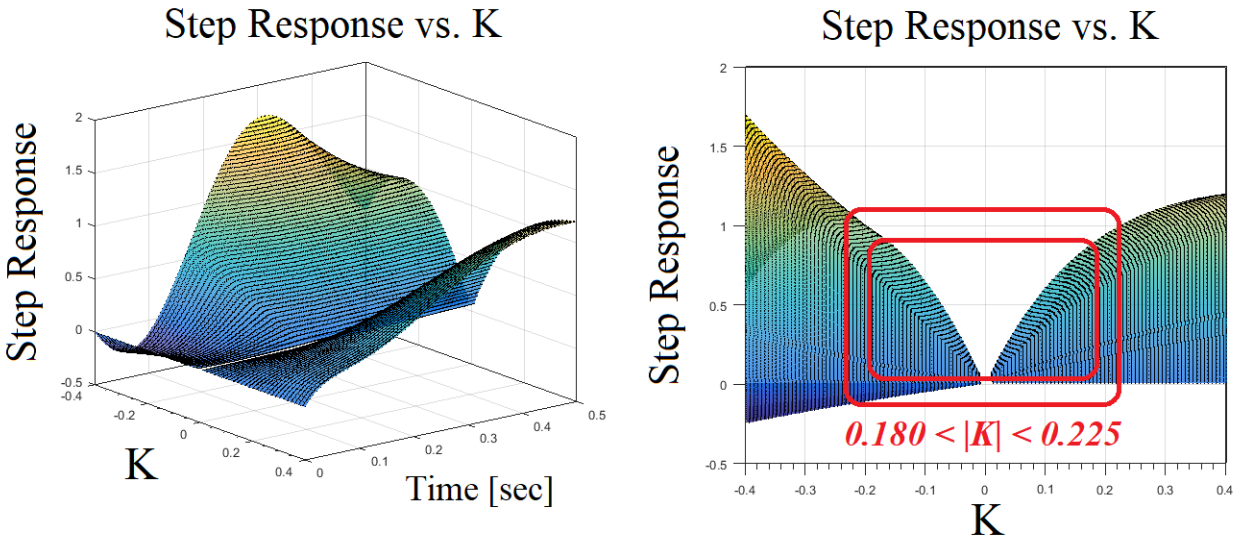

Figure 37: Step response of AP inner loop Vs. $K_{\dot{\theta}} = \pm 0.05$

Finally we arrive at the desired K domain that satisfies the requirement of ($t_r = 10\tau$). In a more traditional SR analysis, presenting the configurations as :

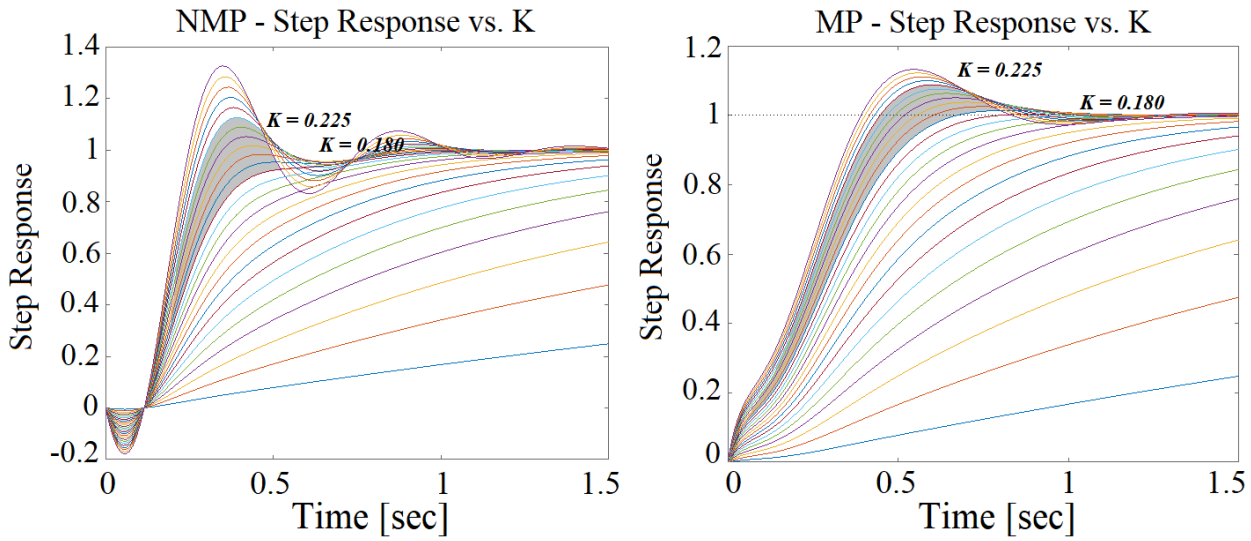

Figure 38: Cross Sectioning of SR for $0.180 < |K| < 0.225$